



**Catalytic activation of ethylene C-H bonds on uniform d8  
Ir(I) and Ni(II) cations in zeolites: toward molecular level  
understanding of ethylene polymerization on heterogeneous  
catalysts**

Journal:	<i>Catalysis Science &amp; Technology</i>
Manuscript ID	CY-ART-07-2019-001442.R2
Article Type:	Paper
Date Submitted by the Author:	15-Oct-2019
Complete List of Authors:	Jaegers, Nicholas; Pacific Northwest National Laboratory, Institute for Integrated Catalysis Khivantsev, Konstantin; Pacific Northwest National Laboratory, Institute for Integrated Catalysis Kovarik, Libor; Pacific Northwest National Laboratory, EMSL Klas, Dan; Pacific Northwest National Laboratory, Institute for Integrated Catalysis Hu, Jian Zhi; Pacific Northwest National Laboratory Wang, Yong; Pacific Northwest National Laboratory, Institute for Integrated Catalysis Szanyi, Janos; Pacific Northwest National Laboratory, Institute for Integrated Catalysis

# Catalytic activation of ethylene C-H bonds on uniform d<sup>8</sup> Ir(I) and Ni(II) cations in zeolites: toward molecular level understanding of ethylene polymerization on heterogeneous catalysts

Nicholas R. Jaegers<sup>1,2,&,\*</sup>, Konstantin Khivantsev<sup>1,&,\*</sup>, Libor Kovarik<sup>1</sup> Daniel W. Klas<sup>1</sup>, Jian Zhi Hu<sup>1</sup>, Yong Wang<sup>1,2</sup>, and János Szanyi<sup>1,&,\*</sup>

<sup>1</sup>Institute for Integrated Catalysis, Pacific Northwest National Laboratory Richland, WA 99352 USA

<sup>2</sup>Voiland School of Chemical Engineering and Bioengineering, Washington State University, Pullman, WA 99163 USA

& These authors contributed equally

\*corresponding authors: Nicholas.Jaegers@pnnl.gov, Konstantin.Khivantsev@pnnl.gov, Janos.Szanyi@pnnl.gov

**ABSTRACT:** The homolytic activation of the strong C-H bonds in ethylene is demonstrated, for the first time, on d<sup>8</sup> Ir(I) and Ni(II) single atoms in the cationic positions of zeolites H-FAU and H-BEA under ambient conditions. The oxidative addition of C<sub>2</sub>H<sub>4</sub> to the metal center occurs with the formation of a d<sup>6</sup> metal vinyl hydride, explaining the initiation of the Cossee-Arlman cycle on d<sup>8</sup> M(I/II) sites in the absence of pre-existing M-H bonds. Under mild reaction conditions (80-220°C, 1 bar), the catalytic dimerization to butenes and dehydrogenative coupling of ethylene to butadiene occurs over these catalysts. 1-Butene is not converted to butadiene under the reaction conditions applied. Post-reaction characterization of the two materials reveals that the active metal cations remain site-isolated whereas deactivation occurs due to the formation of carbonaceous deposits on the zeolites. Our findings have significant implications for the molecular level understanding of ethylene conversion and the development of new ways to functionalize C-H bonds under mild conditions.

Zeolite-supported transition metals (single atoms, clusters, nanoparticles, etc.) represent an important class of materials with uses in the chemical industry, emissions controls, and as model systems to derive structure-function properties in catalysis.<sup>1-9</sup> Among them, d<sup>8</sup> metals such as Ni(II), Rh(I), Ir(I), Pt(II), and Pd(II) have been the focus of many studies to better understand the genesis, speciation, and stability of such species for reactions such as hydrogenations, oxidations, as well as ethylene transformation (di- and oligomerization to butenes and higher oligomers).<sup>10-13</sup> For example, it was shown first in the 1950s that Rh(I)(CO)<sub>2</sub> and Ir(I)(CO)<sub>2</sub> species can be stabilized on oxide supports<sup>14-15</sup> and are active for ethylene conversion to butenes at room temperature, retaining their site-isolated nature after catalysis.<sup>16-18</sup>

The Rh ligand environment is tunable and hydrogen promotes butene formation despite not directly participating in the dimerization reaction (i.e., 2C<sub>2</sub>H<sub>4</sub> → C<sub>4</sub>H<sub>8</sub>).<sup>12, 17-18</sup> This effect was explained in some studies by H<sub>2</sub> enhancing butene desorption on (Rh(C<sub>2</sub>H<sub>4</sub>)<sub>2</sub>/HY).<sup>16</sup> Recently, however, the hydrogen partial pressure dependence of ethylene dimerization was systematically measured on Rh(CO)<sub>2</sub>, Rh(CO)(C<sub>2</sub>H<sub>4</sub>), Rh(CO)(H),<sup>17</sup> and Rh(NO)<sub>2</sub><sup>12</sup> complexes supported on HY zeolites. Positive reaction orders of ~0.7-1 confirmed that hydrogen indeed promotes dimerization, where H<sub>2</sub> was shown to improve the rate of ethylene dimerization up to ~10 fold.<sup>12,17</sup> This was attributed to the formation of metal-hydride-supported species (observed and characterized experimentally<sup>12,17,18</sup>) which provide a low-energy pathway for dimerization via facile insertion of pi-coordinated ethylene into the M-H bond to form an M-Ethyl

moiety which subsequently migrates into another pi-coordinated ethylene to form a Rh-Butyl species prior to facile β-H abstraction to produce butene-1.<sup>12</sup> This attribution was subsequently supported for ethylene dimerization on Ni/BEA, although Ni-H species were not observed directly.<sup>19</sup> Until now, it remained unclear how ethylene, in the absence of M-hydride species, can polymerize considering the importance of M-H intermediates in the Cossee-Arlman mechanism. Theoretical studies have identified potential mechanisms for ethylene dimerization on Ni/BEA where the metallocycle, proton-transfer, and Cossee-Arlman mechanisms were compared.<sup>20</sup> Also considered was the non-catalytic formation of a nickel vinyl intermediate via the heterolytic activation of a C-H bond over Ni(II)-O bond followed by the formation of an active Ni center.<sup>20</sup>

In this study, we demonstrate: 1). Preparation and characterization of highly uniform d<sup>8</sup> metal species. Ni(II) was selected because it has been a challenge to prepare well-defined uniform Ni-zeolite species. We have previously prepared d<sup>8</sup> Pt(II) and Pd(II) species<sup>9</sup> in zeolite uniformly and thus transferred this approach to a Ni/BEA system in order to unravel detailed structure catalytic-property relationships for the historically important system for ethylene polymerization. We also employ the well-defined square planar d<sup>8</sup> Ir(I)(CO)<sub>2</sub> complex anchored in zeolite FAU (like Ni(II)/FAU) because it grafts uniformly in zeolite and also has CO groups which, due to their high molar extinction coefficients and well-resolved nature, allow us to observe ligand changes with enhanced resolution. 2). We obtain the reactivity for ethylene couplings on those materials, showing similar trends for both d<sup>8</sup> metals 3). We resolve a longstanding uncertainty in heterogeneous ethylene polymerization, one of the largest catalytic processes. Though supported metal ions (d<sup>8</sup> like Ni(II), Ir(I), Pd(II) or d<sup>4</sup> Cr(II) perform this reaction without the initiator/co-catalyst, the mechanism for ethylene polymerization initiation and the relevant intermediates involved have remained elusive for the last 50 years. We resolve these uncertainties using state-of-the-art infrared studies supported by microscopy and solid-state NMR measurements<sup>21</sup> for d<sup>8</sup> metal cations on solid supports. In short, ethylene polymerization starts with the homolytic activation of the C-H bonds of ethylene on extremely electrophilic d<sup>8</sup> M sites, resulting in the formation of d<sup>6</sup> metal vinyl hydride complexes which further react with ethylene to form a vinyl ethyl d<sup>6</sup> metal fragment. From this fragment, 1-butene can form either via direct reductive elimination or a Cossee-Arlman type step involving alkyl chain growth through alkyl migration and insertion into M-ethylene bonds.

Though reported for other d<sup>8</sup> metals, it is not straightforward to generate uniform Ni(II) species since they may graft to both silanol nests and various extra-framework zeolite positions, evidenced by IR spectroscopy of CO adsorption.<sup>19</sup> This brought

into question the true active center for ethylene oligomerization activity.<sup>22</sup> To better understand the active centers for ethylene dimerization, well-defined supported complexes of Ir(I) and Ni(II) were generated, characterized, and tested in this study. These active centers not only demonstrate activity to butenes, but butadiene as well; a notable result since 1,3-butadiene is a high-value commodity chemical (~10 million tons per annum) that serves as a precursor to a wide range of plastics and polymers. These reactions proceed via activation of C-H bonds of ethylene on a super electrophilic cationic metal center recently observed for a metal/zeolite system.<sup>23</sup>

A modified IWI method was previously used to produce atomically dispersed Pt and Pd in SSZ-13.<sup>9</sup> We slightly altered this procedure to synthesize 0.4 wt% Ni on BEA by reacting aqueous nickel nitrate with excess ammonia to produce a mononuclear Ni hexamine complex. This mitigates the formation of hydroxo-bridged Ni complexes, which are precursors to NiO nanoparticles, similar to the aqueous solution of Pd(NO<sub>3</sub>)<sub>2</sub> that has the propensity to darken and form ...-OH-Pd-OH-Pd-OH-... networks over time, even in acidic solutions.<sup>9, 24-25</sup> The micropores of BEA zeolite (Si/Al ~ 12.5) were impregnated with this complex, dried in ambient air, and calcined at 550°C in static air. Infrared spectroscopy of adsorbed CO on this material substantiates the exclusive formation of 1 type of Ni(II)-CO in BEA zeolite. The C-O stretching vibrational band of this species is located at 2,211 cm<sup>-1</sup> (Figure 1A).

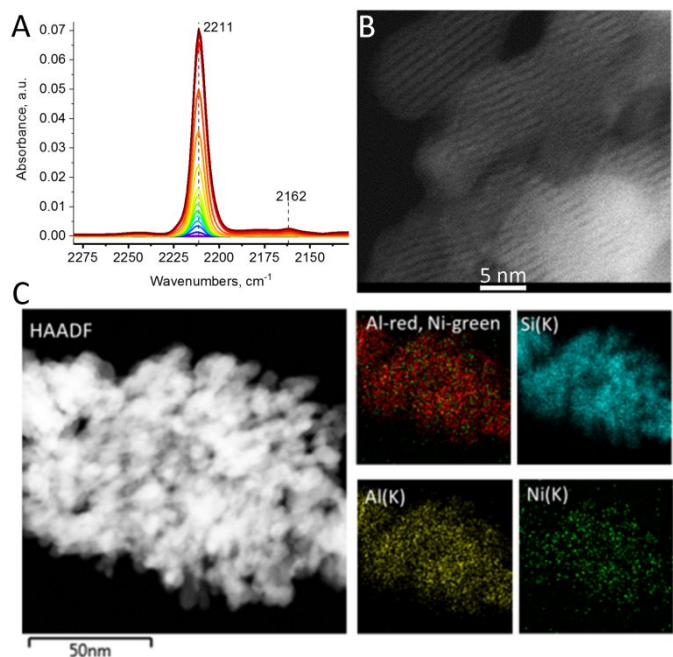


Figure 1. A). FTIR during CO adsorption on dry 0.4% Ni/BEA, P(CO)<sub>max</sub>=5 Torr (the band at 2162 cm<sup>-1</sup> represents adsorbed <sup>13</sup>CO molecules) B). High-resolution HAADF-STEM image of the 0.4% Ni/BEA material: straight channels in BEA nanocrystals are clearly imaged. No NiO clusters or particles observed (additional HAADF-STEM images provided in Figure S2) C). EDS mapping of Ni, Al, Si, and Ni/Al overlay in 0.4% Ni/BEA.

No NiO clusters or nanoparticles could be observed in the channels of BEA. EDS mapping confirmed the presence of Ni associated with BEA, corroborating the presence of uniform,

isolated Ni sites in the sample (Fig. 1B and C, Figure S1-S3). Comprehensive interconversion maps of Ni(II)-CO, Ni(II)-NO, Ni(II)-C<sub>2</sub>H<sub>4</sub>, and Ni(II)(NO)(CO) complexes, never prepared through classical organometallic routes are discussed and available in the Supporting Information (Figure S4-S17). These provide new insight into the Ni/Zeolite chemistry complementary to the previous pioneering studies of Petkov et al.<sup>26</sup> In particular, a new phenomenon in solid supported systems is identified whereby low-temperature CO adsorption produces 2 peaks at 2,214 and 2,204 cm<sup>-1</sup> (Figure S11), that do not belong to the Ni(II)(CO)<sub>2</sub> dicarbonyl complex (evidenced by their contrasting interactions with C<sub>2</sub>H<sub>4</sub> and stability under vacuum, Figs. S12, S13). However, CO adsorption at room temperature produces only 1 band at 2,211 cm<sup>-1</sup>. This indicates that at low temperatures, distinctive Al T-sites exist while at room temperature these sites become degenerate, possibly due to the flexibility of the zeolite framework or relativistic effects, revealing only the 2,211 cm<sup>-1</sup> feature from CO adsorption on super electrophilic Ni(II)/2Al centers.

Unlike Rh(I)/FAU complexes, for which initial ligand environment impacts ethylene dimerization,<sup>12, 17-18</sup> both Ni(II)-CO and Ni(II)-NO undergo ligand replacement by ethylene to form Ni(II)-C<sub>2</sub>H<sub>4</sub> complex under ambient conditions and lower temperatures (Figure S5, S9, S13-S15). This material was active for ethylene transformation to butenes, demonstrating that Ni(II) in the ion-exchange position is active for catalysis (Table S1). Remarkably, 80°C was sufficient to observe activity for both butadiene as well as butenes (1-butene as well as cis- and trans-2-butene) formation. Selectivity initially favored butadiene at 120°C (~65%, TOF ~122 hr<sup>-1</sup> with respect to butadiene formed and ~240 hr<sup>-1</sup> with respect to ethylene molecules reacted, Table S1), however, selectivity quickly dropped to ~10% within the first 30 minutes (TOF ~ 10 hr<sup>-1</sup>). Above 180°C, activity for butadiene production is enhanced with selectivity around 20-30% on a molar basis at 200°C and initial TOF ~200 hr<sup>-1</sup>. Even at elevated temperatures, deactivation is observed both for butene and butadiene production with time on stream (Figure S18).

These results are noteworthy since C-H bond activation in ethylene (22 kJ/mol stronger than methane at 298K) is a challenging catalytic step. Accordingly, functionalization of ethylene typically involves reactions with its C=C bond and not the C-H bond directly. By activating the C-H bond in ethylene, the formal coupling of two vinyl C<sub>2</sub>H<sub>3</sub> fragments enables the formation of butadiene.

Catalytically, butadiene can be produced by dehydrogenation of n-butane and 1-butene (Houdry process) or by ethanol conversion to butadiene, hydrogen, and water over a mixed metal oxide catalyst (Lebedev and Ostromyslenski process). These catalytic processes with unpromoted catalysts produce butadiene unselectively and are energy intensive (400-700°C).<sup>27</sup> The best current processes based on ethanol show excellent selectivity to butadiene for promoted materials (>90%) whereas the unpromoted, historically important Ta-containing material has a selectivity of ~15%. However, this process relies on a low ethanol feed rate (GHSV), features turnovers of ~ 1 hr<sup>-1</sup> at 320°C, and suffers deactivation due to formation of polymeric carbonaceous deposits.<sup>28-29</sup>

Though pathways from alcohol feedstocks exist, the catalytic conversion of ethylene to butadiene remains effectively unprecedented with just a few examples proposed. In 1983, (C<sub>5</sub>(CH<sub>3</sub>)<sub>5</sub>)<sub>2</sub>Ti(C<sub>2</sub>H<sub>4</sub>) complexes in aromatic solvents were suggested to convert ethylene into 1,3-butadiene and ethane at 25°C and ~4 atm in a sealed batch reactor, though the reported TOF after one year was ~1-2 year<sup>-1</sup>, rendering catalysis

indeterminate.<sup>30</sup> Notably, in 2015 ethylene has been selectively converted to butadiene over FAU-supported  $\text{Rh}(\text{CO})_2$  and  $\text{Rh}(\text{CO})(\text{C}_2\text{H}_4)$  single-atom catalysts at 25°C and 1 atm under continuous ethylene flow, yielding a TOF of  $\sim 2 \text{ hr}^{-1}$ ,<sup>17</sup> marking the discovery of the dehydrogenative coupling of ethylene into butadiene ( $2\text{C}_2\text{H}_4 \rightarrow \text{C}_4\text{H}_6 + \text{H}_2$ ). In 2018, an  $\text{Ir}(\text{C}_2\text{H}_4)_2(\text{Phebox})$  organometallic complex was shown to convert ethylene catalytically via  $3\text{C}_2\text{H}_4 \rightarrow \text{C}_4\text{H}_6 + \text{C}_2\text{H}_6$  with butene by-products [ $\text{S}_{\text{C}_4\text{H}_6} < 45\%$ ; P: 2–12 atm; TOF:  $0.25 \text{ hr}^{-1}$  at 2 atm/100°C,  $0.9 \text{ hr}^{-1}$  at 12 atm/110°C].<sup>31</sup> Despite this progress, the catalytic chemistry of butadiene formation from a cheap ethylene feedstock under mild conditions remains unattained, demonstrating the relevance of the observed butadiene activity at 120°C for Ni/BEA. We note that fast deactivation at this temperature is not surprising considering that H-zeolites are often used as butadiene adsorbents.<sup>32</sup>

After catalysis, exposure of the sample to CO restores the original  $2,211 \text{ cm}^{-1}$  feature (Figure S16–S17), but to a lesser extent due to unsaturated carbonaceous deposits blocking the active sites, further confirmed by *in situ*  $^{13}\text{C}$  NMR (Figure S24).<sup>33</sup> The absence of vibrational signatures for Ni(I) and Ni(0) carbonyl complexes further suggests that no reduction of Ni(II) occurred during ethylene dimerization and that Ni(II) in the ion-exchange positions of the zeolite is the active site in ethylene dimerization (Figure S17).

Moreover, post-reaction (200°C in ethylene flow) CO adsorption reveals a peak around  $\sim 2,230 \text{ cm}^{-1}$  (Figure S16–17) not present in the fresh sample. This corresponds to CO adsorbed on extraframework aluminium<sup>34</sup> formed under mild catalytic conditions in the presence of Ni(II) atoms and ethylene. Solid-state NMR further confirms this result via comparison of  $^{27}\text{Al}$  MAS NMR spectra of fresh and spent samples (Figure S19) which show that dealumination indeed occurs under mild conditions, evidenced by a feature at  $\sim 30 \text{ ppm}$  due to the presence of penta-coordinate extraframework Al sites as well as broadening of tetrahedral Al bands. Such mild conditions have been not previously reported to cause dealumination of the zeolite framework. This is likely due to polymerization of ethylene in the microporous channels and the subsequent breakage of pores.

In addition to the supported  $d^8$  Ni(II) species, a 0.7 wt%  $\text{Ir}(\text{CO})_2$  species was prepared on H-FAU zeolite with Si/Al  $\sim 15$  as for Ni/BEA. This formulation was previously characterized with EXAFS and FTIR,<sup>35</sup> where its interaction with ethylene was reported to produce  $\text{Ir}(\text{CO})(\text{C}_2\text{H}_4)$  complexes. Pulses of ethylene, followed by inert gas purging indeed produce only the  $\text{Ir}(\text{CO})(\text{C}_2\text{H}_4)$  complex in this study (Figure 2A,C).

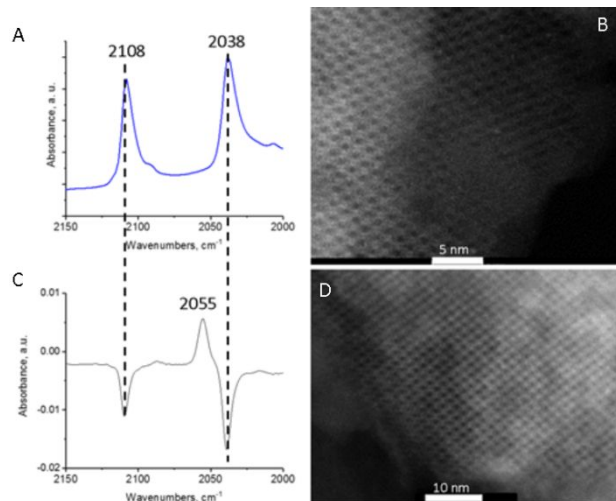


Figure 2. A). DRIFTS spectrum of the starting 0.7%  $\text{Ir}(\text{CO})_2/\text{FAU}$  Si/Al $\sim 15$  material B). High-resolution HAADF-STEM image of the fresh Ir/FAU in [110] projection, individual Ir atoms can be seen in the supercycles C). DRIFTS difference spectrum during reaction of  $\text{Ir}(\text{CO})_2/\text{FAU}$  with pulses of dilute ethylene, showing disappearance of  $2,108$  and  $2,038 \text{ cm}^{-1}$  bands of  $\text{Ir}(\text{CO})_2$  and appearance of only 1 new band at  $2,055 \text{ cm}^{-1}$ , belonging to  $\text{Ir}(\text{CO})(\text{C}_2\text{H}_4)/\text{FAU}$  complex. D). High-resolution HAADF-STEM image of  $\text{Ir}(\text{CO})_2/\text{FAU}$  after ethylene catalysis at 225°C for 1 hour, in the [110] projection, showing lack of Ir agglomeration.

DRIFTS confirms the successful grafting of the complex with the formation of symmetric and asymmetric CO stretches of the square-planar  $\text{Ir}(\text{CO})_2$  fragment at  $2,108$  and  $2,038 \text{ cm}^{-1}$ .<sup>12,17,18</sup> HAADF-STEM imaging (Figure S20, 2B) further confirms site-isolated nature of the complex in the zeolite micropores. Sample exposure to flowing pure  $\text{C}_2\text{H}_4$  in the DRIFTS cell revealed transient behavior (Figure 3).

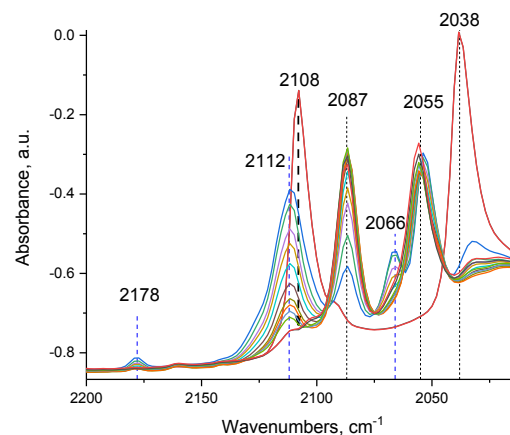
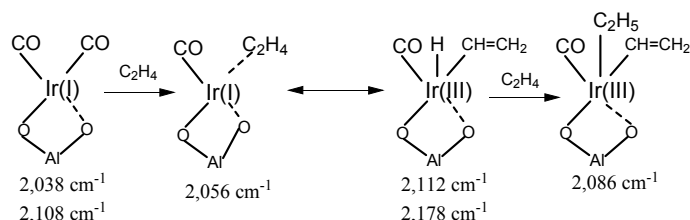


Figure 3. DRIFTS spectrum of 0.7%  $\text{Ir}(\text{CO})_2/\text{FAU}$  Si/Al $\sim 15$  during exposure to flowing pure ethylene (the first 5 minutes).



The peaks, belonging to the symmetric and asymmetric CO stretches of  $\text{Ir}(\text{CO})_2$ , at 2,108 and 2,038  $\text{cm}^{-1}$  declined while new features emerged. The 2,055  $\text{cm}^{-1}$  feature has been previously assigned to the  $\text{Ir}(\text{CO})(\text{C}_2\text{H}_4)$  complex<sup>12,17,18</sup>; however, careful inspection of the spectra in the 2,060 – 2,030  $\text{cm}^{-1}$  region reveals new features (Figure 4): the 2,066 and 2,053  $\text{cm}^{-1}$  peaks decrease in concert as the 2,056  $\text{cm}^{-1}$  feature of  $\text{Ir}(\text{CO})(\text{C}_2\text{H}_4)$  grows with clear isosbestic points (shaded).

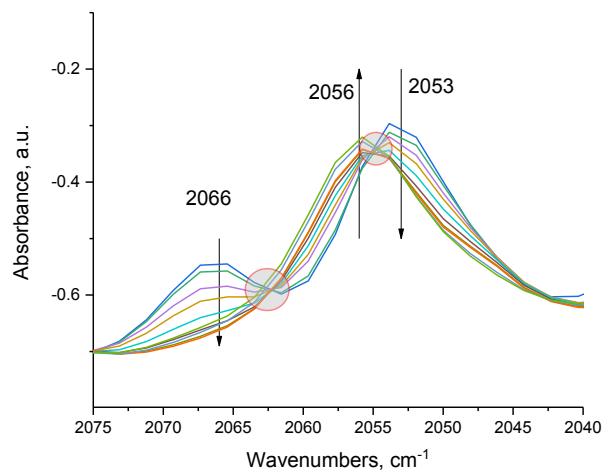
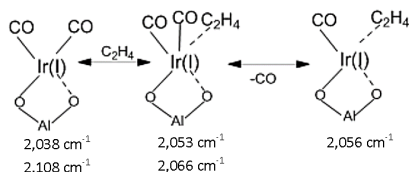


Figure 4. DRIFTS spectrum of 0.7%  $\text{Ir}(\text{CO})_2/\text{FAU Si/Al}\sim 15$  during exposure to flowing ethylene (initial 5 minutes).

This indicates the stoichiometric transformation of  $\text{Ir}(\text{CO})_2$  into  $\text{Ir}(\text{CO})(\text{C}_2\text{H}_4)$ , occurring via the following sequence:



Initially, the square-planar  $\text{Ir}(\text{CO})_2$  accepts one  $\text{C}_2\text{H}_4$  ligand to form a  $\text{Ir}(\text{CO})_2(\text{C}_2\text{H}_4)$  species which then expels one CO ligand, forming square-planar  $\text{Ir}(\text{CO})(\text{C}_2\text{H}_4)$ . Concomitantly bands at 2,178  $\text{cm}^{-1}$  (weak) and 2,112  $\text{cm}^{-1}$  (intense) develop within the first 1 minute of ethylene exposure (Figure 5).

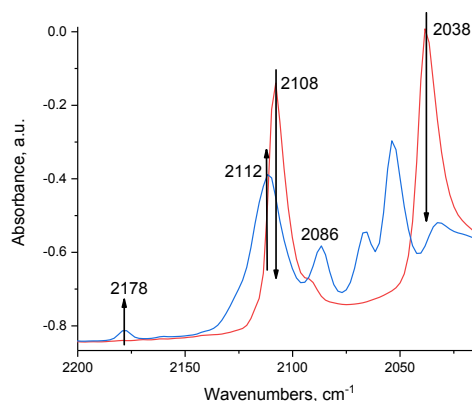


Figure 5. DRIFTS spectrum of 0.7%  $\text{Ir}(\text{CO})_2/\text{FAU Si/Al}\sim 15$  during exposure to ethylene (~1 minute). 2,178 and 2,112  $\text{cm}^{-1}$  grow in concert.

The intense 2,112  $\text{cm}^{-1}$  band belongs to the CO vibration of an oxidized Ir center (CO adsorbed on metal cations has high molar extinction coefficients) and the low intensity 2,178  $\text{cm}^{-1}$  band corresponds to the Ir-H stretching vibration. Indeed, this fully agrees with the described synthesis of the first supported, transition metal carbonyl hydride complexes of  $\text{Rh}(\text{III})(\text{H})_x(\text{CO})_y$  and relatively low intensity of Rh-H stretching vibrations compared to CO vibrations.<sup>17,18</sup> We note that Rh(III) and Ir(III) have the same  $d^6$  electronic configuration and provide the analogous (to Rh) synthesis of Ir(III) carbonyl hydride complex,<sup>18</sup> unambiguously identifying the Ir-H stretch at 2,150  $\text{cm}^{-1}$ . Analogous to the selective synthesis of  $\text{Rh}(\text{III})(\text{CO})\text{H}_2$  complexes from  $\text{Rh}(\text{CO})_2$ ,<sup>18</sup> the  $\text{Ir}(\text{CO})\text{H}_x$  species has been suggested from treatments of  $\text{Ir}(\text{CO})_2/\text{FAU}$  with ethylene followed by hydrogen.<sup>35</sup> In that study, the authors failed to identify the Ir-H stretch, concluding that its signature is too weak to be observed. We treated our  $\text{Ir}(\text{CO})_2$  materials with  $\text{C}_2\text{D}_4$ , forming first  $\text{Ir}(\text{I})(\text{CO})(\text{C}_2\text{D}_4)$  which we then exposed to  $\text{H}_2$  flow (Figs. S29, S30, S31). Both the actual spectra and difference spectra indicate selective conversion of  $\text{Ir}(\text{CO})(\text{C}_2\text{D}_4)$  to the  $\text{Ir}(\text{CO})(\text{H})_2$  complex with CO stretching observed at 2,065  $\text{cm}^{-1}$  and the Ir-H stretch at 2,150  $\text{cm}^{-1}$ . Isotopic shift experiments with  $\text{D}_2$  (Fig. S31) confirm that the 2,150  $\text{cm}^{-1}$  is indeed the Ir-H stretch.

As such, the simultaneous formation of new Ir-H and Ir-CO stretches (Figs. 5 and 6) arises from the generation of one species. The high-lying stretch of Ir-CO means that Ir is in the +3 oxidation state, signifying the unprecedented oxidative addition of the C-H bonds of ethylene to the  $\text{Ir}(\text{CO})$  fragment with the formation of  $\text{Ir}(\text{III})(\text{CO})(\text{H})(\text{C}_2\text{H}_3)$  carbonyl vinyl hydrido-complex:  $\text{C}_2\text{H}_4\text{-Ir}(\text{I})\text{-CO} \leftrightarrow \text{C}_2\text{H}_3\text{-Ir}(\text{III})(\text{H})(\text{CO})$ . These assignments and described behavior are further supported by observation of these species the in situ NMR data (Figure S23).

As the concentration of this complex reaches its maximum (~1 minute), the intensities of both the 2,112 and 2,178  $\text{cm}^{-1}$  features reach their maxima and then decline in concert as a new CO stretching band develops at 2,086  $\text{cm}^{-1}$  that has no corresponding Ir-H stretching band (Figure 6). This indicates the hydride is consumed during the reaction with ethylene. This suggests the consequent formation of an  $\text{Ir}(\text{III})(\text{CO})(\text{C}_2\text{H}_5)(\text{C}_2\text{H}_3)$  complex via ethylene insertion into the Ir-H bond.

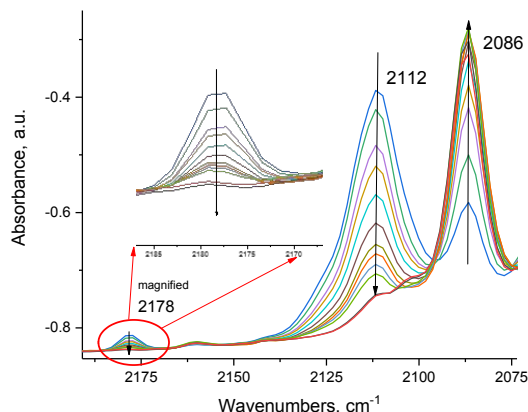


Figure 6. DRIFTS spectrum of 0.7% Ir(CO)<sub>2</sub>/FAU during exposure to ethylene (~5 minutes). The 2,112 and 2,178 cm<sup>-1</sup> bands decline simultaneously as the 2,087 cm<sup>-1</sup> feature grows.

Furthermore, in order to unambiguously assign the 2,178 cm<sup>-1</sup> band to the Ir-H stretch, we replicated the infrared experiment on Ir(CO)<sub>2</sub> and C<sub>2</sub>H<sub>4</sub> with C<sub>2</sub>D<sub>4</sub>. We observed the absence of the 2,178 cm<sup>-1</sup> band (Ir-H stretch), upon oxidative addition of C<sub>2</sub>D<sub>4</sub> to the Ir(I) center. Instead, Ir(III)-D species forms (Fig. S32).

The observed room-temperature activation of C-H bonds with the formation of iridium carbonyl alkyl hydride complex is unprecedented. Such transformation have been only rarely described in organometallic literature<sup>36</sup> and never directly observed spectroscopically on any solid material. The bond is not split heterolytically on the M-O bond but instead it is activated homolytically via oxidative addition to an electrophilic d<sup>8</sup> metal center in the zeolite micropore. High coordinative unsaturation and superelectrophilicity of M cations in zeolite have been recently quantified for isoelectronic d<sup>8</sup> Pd(II) ions,<sup>23</sup> explaining why this reaction is favored over heterolytic activation of C-H bonds on covalent M-O bond. It is important to note that such a homolytic pathway of C-H bond activation has been previously overlooked in the metal/zeolite and M/oxide literature. Indeed, heterolytic activation of strong X-H bonds (C-H of hydrocarbons and N-H of ammonia) normally require relatively high temperatures.<sup>37-38</sup>

Ethylene activity over Ir(CO)<sub>2</sub>/FAU produces measurable amounts of butenes at temperatures above 80°C and butadiene at temperatures above 180 °C with the maximum rate of catalytic butadiene production at ~200-220°C and selectivities to butadiene on the order 17-20% (Table S 2). After catalysis, Ir remains site-isolated and does not agglomerate into Ir nanoparticles as evidenced by HAADF-STEM and FTIR data (Figure 2D, S21, S22). Formation of carbonaceous polymeric deposits, framework breakage, and dealumination similar to Ni/BEA is also observed (Figs. S20, S21, S25). The ease with which oxidative addition of ethylene C-H bond to highly electrophilic Ir(I) center takes place at room temperature at 1 bar pressure of ethylene, suggests that C-H activation is not the rate-limiting step of the ethylene dimerization under these conditions: C-C coupling and/or beta-hydride elimination are expected to be rate-limiting steps in catalysis.

We construct two plausible catalytic pathways for butadiene (and butene) production. Two different steps of initial C-H bond activation are possible: 1) homolytic activation of C-H bond via oxidative addition to M d<sup>8</sup> center, which we observe

experimentally (Figure S26) and 2) heterolytic activation of C-H bond on the M-Ozeolite pair (Figure S27), which we did not observe. Two ethylene molecules could also couple on single d<sup>8</sup> metal center with the formation of metallacyclopentane species (Figure S28), that were shown by Goldman and co-workers to form on Ir(C<sub>2</sub>H<sub>4</sub>)<sub>2</sub>(Phebox) system by trapping via CO.<sup>31</sup> The stability of the species, as noted previously by Halpern,<sup>39</sup> does not mean that it is the true active state of the catalyst. Indeed, most active species are formed transiently (as we observe experimentally for Ir(III)(H)(CO)(C<sub>2</sub>H<sub>3</sub>) species), hence mechanism in Fig. S26 is most likely operative.

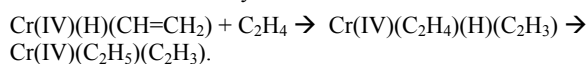
Furthermore, deeper mechanistic insight into the pathway of butadiene production was achieved by refuting the direct dehydrogenation of butene into butadiene. When 1-butene was introduced to the catalyst at 150-200°C, no butadiene was observed. Thus, the route to butadiene mechanistically differs from direct butene dehydrogenation. Indeed, such dehydrogenation does not take place on single Ir atoms under such mild conditions.

Notably, in the most probable reaction mechanism depicted in Fig. S26, we propose 1-butene formation directly from Ir(III)(CO)(C<sub>2</sub>H<sub>3</sub>)(C<sub>2</sub>H<sub>3</sub>) and Ni(IV)(C<sub>2</sub>H<sub>3</sub>)(C<sub>2</sub>H<sub>3</sub>) via reductive elimination of the ethyl and vinyl fragments with restoration of Ni(II) and Ir(I)-CO fragments which reform Ni(II)(C<sub>2</sub>H<sub>4</sub>) and Ir(I)(CO)(C<sub>2</sub>H<sub>4</sub>) in the presence of ethylene. It is also possible that beta-hydride elimination releases 1-butene from the M-(n-Butyl) intermediate, which forms when the ethyl group in M(C<sub>2</sub>H<sub>4</sub>)(C<sub>2</sub>H<sub>3</sub>) migrates. Butadiene may be formed analogous to this scheme but in this case the vinyl group of M(C<sub>2</sub>H<sub>3</sub>)(C<sub>2</sub>H<sub>4</sub>) fragment migrates, forming M-CH<sub>2</sub>-CH<sub>2</sub>-CH=CH<sub>2</sub>, from which via beta-hydride elimination butadiene-1,3 is released.

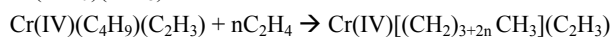
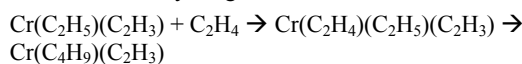
These findings for supported Ni(II) and Ir(I) isolated sites may help reveal mechanistic uncertainties for the Cr/SiO<sub>2</sub> Phillips ethylene polymerization catalyst, extensively studied over 50 years. Though believed to follow a Cossee-Arlman Cr-alkyl mechanism, the low number of active sites (<10%), amorphous silica support, fast reaction rates, and the presence of multiple oxidation states of Cr prevented a thorough understanding of the initiation mechanism. Recent elegant studies<sup>40</sup> demonstrated that Cr(II) sites are required to start ethylene polymerization, and earlier kinetic studies suggested schemes consistent with activation of ethylene on Cr(II) sites to form Cr(IV) vinyl hydride,<sup>41-42</sup> though this species has never been observed. Based on our current findings, we suggest that the active fraction of the catalyst could be the highly electrophilic Cr(II) species that can add ethylene via C-H oxidative addition to form a Cr(IV)-vinyl (C<sub>2</sub>H<sub>3</sub>)-hydride (H) species:



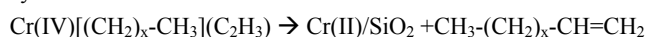
The formation of Cr-ethyl follows:



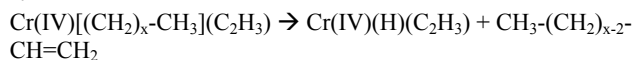
Cr(IV)(C<sub>2</sub>H<sub>5</sub>)(C<sub>2</sub>H<sub>3</sub>) sites may facilitate longer alkyl chain formation via alkyl migration:



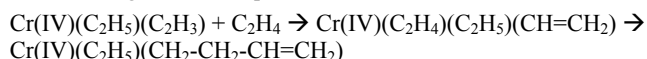
Subsequently, direct reductive elimination of CH<sub>3</sub>(CH<sub>2</sub>)<sub>x</sub>CH=CH<sub>2</sub> is possible which restores the Cr(II) site and re-starts the catalytic cycle:



Beta-hydride elimination from Cr(IV)[(CH<sub>2</sub>)<sub>x</sub>-CH<sub>3</sub>](C<sub>2</sub>H<sub>3</sub>) could also restore Cr(IV)(H)(C<sub>2</sub>H<sub>3</sub>) and re-start the polymerization cycle:



The proposed mechanism does not contradict experimental observations and provides a plausible explanation for the initiation uncertainties of the Phillips catalyst. Furthermore, support for this proposed mechanism is obtained from recent works, in which -CH<sub>2</sub>-CH<sub>2</sub>-CH=CH<sub>2</sub> sites were suggested to form on the catalyst.<sup>43</sup> These sites can form from the vinyl migration in the following reaction sequence:



In conclusion, we provide the first experimental mechanistic evidence of how ethylene dimerization occurs and proceeds on d<sup>8</sup> M(I and II) cations in zeolites in the absence of an initial M-H species: the M-H bond is formed via the homolytic activation of ethylene's C-H bond (stronger than that of methane) on very electrophilic Ir(I) sites in the zeolite micropore. Further, the preparation of well-defined Ir(I) and Ni(II) d<sup>8</sup> in zeolites is demonstrated and accompanied by new chemistry and characterization for both systems before and after catalysis. Both Ni(II) and Ir(I) in zeolites produce butenes and, unprecedentedly, butadiene upon reaction with ethylene under mild conditions. Notably, Ni is more active at lower temperatures toward C-H bond activation than the expensive Ir.

## ACKNOWLEDGMENTS

The research described in paper is part of the Quickstarter Initiative at Pacific Northwest National Laboratory. It was conducted under the Laboratory Directed Research and Development Program at PNNL, a multiprogram national laboratory operated by Battelle for the U.S. Department of Energy. The research described in this paper was performed in the Environmental Molecular Sciences Laboratory (EMSL), a national scientific user facility sponsored by the DOE's Office of Biological and Environmental Research and located at the Pacific Northwest National Laboratory (PNNL). PNNL is operated for the US DOE by Battelle (DE-AC06-76RLO 1830, DE-AC05-RL01830, FW-47319).

## Notes

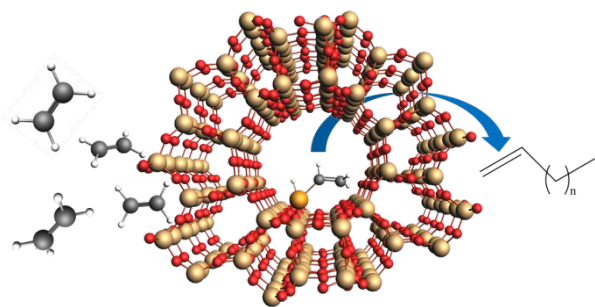
The authors declare no competing financial interests.

## REFERENCES

- Sachtler, W. M. H., *Catal Today* **1992**, *15* (3-4), 419-429.
- Klier, K., *Langmuir* **1988**, *4* (1), 13-25.
- Lonyi, F.; Kovacs, A.; Szegedi, A.; Valyon, J., *J Phys Chem C* **2009**, *113* (24), 10527-10540.
- Corma, A.; Garcia, H., *Topics in Catalysis* **2008**, *48* (1-4), 8-31.
- Haruta, A., *Chemical Record* **2003**, *3* (2), 75-87.
- Barrer, R., Surface Organometallic Chemistry: Molecular Approaches to Surface Catalysis. In *Zeolite Synthesis: An Overview*, Basset, J.-M.; Gates, B. C.; Candy, J.-P.; Choplin, A.; Leconte, M.; Quignard, F.; Santini, C., Eds. Kluwer Academic Publishers: 1988; pp 221-244.
- Kwak, J. H.; Tran, D.; Burton, S. D.; Szanyi, J.; Lee, J. H.; Peden, C. H. F., *J Catal* **2012**, *289*, 272-272.
- Sachtler, W. M. H., *Accounts of Chemical Research* **1993**, *26* (7), 383-387.
- Khivantsev, K.; Jaegers, N. R.; Kovarik, L.; Hanson, J. C.; Tao, F.; Tang, Y.; Zhang, X. Y.; Koleva, I. Z.; Aleksandrov, H. A.; Vayssilov, G. N.; Wang, Y.; Gao, F.; Szanyi, J., *Angew Chem Int Edit* **2018**, *57* (51), 16672-16677.
- Finiels, A.; Fajula, F.; Hulea, V., *Catal Sci Technol* **2014**, *4* (8), 2412-2426.
- Baiale, J., US Patent: US3738977A 1971.
- Khivantsev, K.; Vityuk, A.; Aleksandrov, H. A.; Vayssilov, G. N.; Blom, D.; Alexeev, O. S.; Amiridis, M. D., *Acs Catal* **2017**, *7* (9), 5965-5982.
- Agirrezabal-Telleria, I.; Iglesia, E., *J Catal* **2017**, *352*, 505-514.
- Yang, A. C.; Garland, C. W., *J Phys Chem-US* **1957**, *61* (11), 1504-1512.
- Knozinger, H.; Thornton, E. W.; Wolf, M., *J Chem Soc Farad T 1* **1979**, *75*, 1888-1899.
- Serna, P.; Gates, B. C., *Angew Chem Int Edit* **2011**, *50* (24), 5528-5531.
- Khivantsev, K. PhD Thesis University of South Carolina, 2015.
- Khivantsev, K.; Vityuk, A.; Aleksandrov, H. A.; Vayssilov, G. N.; Alexeev, O. S.; Amiridis, M. D., *J Phys Chem C* **2015**, *119* (30), 17166-17181.
- Joshi, R.; Zhang, G. H.; Miller, J. T.; Gounder, R., *Acs Catal* **2018**, *8* (12), 11407-11422.
- Brogaard, R. Y.; Olsbye, U., *Acs Catal* **2016**, *6* (2), 1205-1214.
- Jaegers, N. R.; Lai, J. K.; He, Y.; Walter, E.; Dixon, D. A.; Vasiliu, M.; Chen, Y.; Wang, C. M.; Hu, M. Y.; Mueller, K. T.; Wachs, I. E.; Wang, Y.; Hu, J. Z., *Angew Chem Int Edit* **2019**, *131*, 12739-12746.
- Moussa, S.; Concepcion, P.; Arribas, M. A.; Martinez, A., *Acs Catal* **2018**, *8* (5), 3903-3912.
- Khivantsev, K.; Jaegers, N. R.; Koleva, I. Z.; Aleksandrov, H. A.; Kovarik, L.; Engelhard, M.; Gao, F.; Wang, Y.; Vayssilov, G. N.; Szanyi, J., *Chemrxiv* **2019**. DOI: 10.26434/chemrxiv.7789454
- Khivantsev, K.; Jaegers, N. R.; Kovarik, L.; Proding, S.; Derewinski, M. A.; Wang, Y.; Gao, F.; Szanyi, J., *Appl Catal a-Gen* **2019**, *569*, 141-148.
- Khivantsev, K.; Gao, F.; Kovarik, L.; Wang, Y.; Szanyi, J., *J Phys Chem C* **2018**, *122* (20), 10820-10827.
- Petkov, P. S.; Aleksandrov, H. A.; Valtchev, V.; Vayssilov, G. N., *Chemistry of Materials* **2012**, *24* (13), 2509-2518.
- Pomalaza, G.; Capron, M.; Ordonsky, V.; Dumeignil, F., *Catalysts* **2016**, *6* (12).
- Dagle, V. L.; Flake, M. D.; Lemmon, T. L.; Lopez, J. S.; Kovarik, L.; Dagle, R. A., *Appl Catal B-Environ* **2018**, *236*, 576-587.

29. Sushkevich, V. L.; Ivanova, I. I., *Appl Catal B-Environ* **2017**, *215*, 36-49.
30. Cohen, S. A.; Auburn, P. R.; Bercaw, J. E., *Journal of the American Chemical Society* **1983**, *105* (5), 1136-1143.
31. Gao, Y.; Emge, T. J.; Krogh-Jespersen, K.; Goldman, A. S., *Journal of the American Chemical Society* **2018**, *140* (6), 2260-2264.
32. Tsybulevski, A. M.; Kustov, L. M.; Weston, K. C.; Greish, A. A.; Tkachenko, O. P.; Kucherov, A. V., *Industrial & Engineering Chemistry Research* **2012**, *51* (20), 7073-7080.
33. Jaegers, N. R.; Hu, M. Y.; Hoyt, D. W.; Wang, Y.; Hu, J. Z., Development and Application of In Situ High-Temperature, High-Pressure Magic Angle Spinning NMR. In *Modern Magnetic Resonance*, Webb, G. A., Ed. Springer International Publishing: Cham, 2017; pp 1-19.
34. Szanyi, J.; Paffett, M. T., *Microporous Mater* **1996**, *7* (4), 201-218.
35. Martinez-Macias, C.; Serna, P.; Gates, B. C., *Acs Catal* **2015**, *5* (10), 5647-5656.
36. Haddleton, D. M.; Perutz, R. N., *J Chem Soc Chem Comm* **1986**, (23), 1734-1736.
37. Khivantsev, K.; Biancardi, A.; Fathizadeh, M.; Almalki, F.; Grant, J. L.; Tien, H. N.; Shakouri, A.; Blom, D. A.; Makris, T. M.; Regalbuto, J. R.; Caricato, M.; Yu, M., *Chemcatchem* **2018**, *10* (4), 736-742.
38. Hu, B.; Getsoian, A.; Schweitzer, N. M.; Das, U.; Kim, H.; Niklas, J.; Poluektov, O.; Curtiss, L. A.; Stair, P. C.; Miller, J. T.; Hock, A. S., *J Catal* **2015**, *322*, 24-37.
39. Goldman, A. S.; Landis, C. R.; Sen, A., *Angew Chem Int Edit* **2018**, *57* (17), 4460-4460.
40. Morra, E.; Martino, G. A.; Piovano, A.; Barzan, C.; Groppo, E.; Chiesa, M., *J Phys Chem C* **2018**, *122* (37), 21531-21536.
41. Kissin, Y. V.; Brandolini, A. J., *J Polym Sci Pol Chem* **2008**, *46* (16), 5330-5347.
42. Zielinski, P.; Lana, I. G. D., *J Catal* **1992**, *137* (2), 368-376.
43. Chakrabarti, A.; Gierada, M.; Handzlik, J.; Wachs, I. E., *Topics in Catalysis* **2016**, *59* (8-9), 725-739.

TOC



The long-debated intermediates of ethylene polymerization are revealed using uniform  $d^8$  metal ions in zeolites.